SF2A 2014
J. Ballet, F. Bournaud, F. Martins, R. Monier and C. Reylé (eds)

GALAXY CLUSTERS IN THE SDSS STRIPE 82

F. Durret[1], C. Adami[2], E. Bertin[1], J. Hao[3], I. Márquez[4], N. Martinet[1], S. Maurogordato[5], T. Sauvaget[6], N. Scepi[7] and M.P. Ulmer[8]

Abstract.

We have searched for galaxy clusters in the Stripe 82 region of the Sloan Digital Sky Survey with AMACFI (Adami & MAzure Cluster FInder, Adami & Mazure 1999), and applied the same method to the Millennium simulation to estimate our detection efficiency and the approximate masses of the detected clusters. We detected 956 clusters at a 3σ level and above, in the redshift range $0.1 \leq z \leq 0.75$, with estimated mean masses between $\sim 10^{13}$ and a few 10^{14} $M_{\odot}$. Considering all the cluster galaxies (i.e. within a 2 Mpc radius of the cluster to which they belong and with a photo$-z$ differing by less than ± 0.1 from that of the cluster), we stacked clusters in various redshift bins to derive colour–magnitude diagrams and are in the process of deriving galaxy luminosity functions (GLFs).

For each galaxy brighter than $M_r < -19.5$, we computed the disk and spheroid components by applying a new version of SExtractor, and by stacking clusters we determined how the disk to spheroid flux ratio varies with cluster redshift and mass. The percentage of early to late type galaxies in clusters ranges roughly between 40% and 50%, and the fraction of late type to early type galaxies shows a slight increase ($\leq 10\%$) with redshift and a decrease ($\sim 10\%$) with cluster detection level, i.e. cluster mass.

From the properties of their galaxies, the *candidate clusters* detected here seem in majority to be "real" clusters, with typical cluster properties.

Keywords: Clusters of galaxies, SDSS Stripe 82

1 Introduction

The discovery of new galaxy clusters is important for two main reasons. First, clusters are important *per se*, since their detailed analysis allows to understand how galaxies form and evolve in various environments. And second, they play an important part in cosmology, since their number as a function of redshift allows to set constraints on cosmological parameters.

A number of methods is available to detect clusters in imaging surveys, among which AMACFI (Adami & MAzure Cluster FInder, Adami & Mazure 1999). We have applied this method to the CFHTLS Deep and Wide fields (Mazure et al. 2007, Adami et al. 2010, Durret et al. 2011) and recently applied this method to the SDSS Stripe 82 field (Durret et al. 2014, A&A to be submitted).

[1] UPMC Université Paris 06, UMR 7095, Institut d'Astrophysique de Paris, 98bis Bd Arago, F-75014, Paris, France
[2] LAM, OAMP, Université Aix-Marseille & CNRS, Pôle de l'Etoile, Site de Château Gombert, 38 rue Frédéric Joliot-Curie, 13388 Marseille 13 Cedex, France
[3] ETS Corporate Headquarters, 660 Rosedale Road, Princeton, NJ 08541, USA
[4] Instituto de Astrofísica de Andalucía, CSIC, Glorieta de la Astronomía s/n, 18008, Granada, Spain
[5] OCA, Cassiopée, Boulevard de l'Observatoire, B.P. 4229, F-06304 NICE Cedex 4, France
[6] Observatoire de Paris-Meudon, GEPI, 92195 Meudon Cedex, France
[7] ENS-Cachan, 61 avenue du Président Wilson, 94235 Cachan, France
[8] Department of Physics & Astronomy, CIREA, Northwestern University, Evanston, IL 60208-2900, USA

2 The data and method

The SDSS has obtained many scans in the so-called Stripe 82 (hereafter S82) field, defined by right ascension approximately in the range $310° - 59°$ and declination $|\delta| < 1.25°$ (J2000). Five photometric bands are available: u, g, r, i, and z.

We started with a catalogue of 13,621,718 objects, with positions, magnitudes and photometric redshifts (hereafter photo$-z$s), made by Reis et al. (2012). This catalogue is limited in magnitude to $i < 23$. To avoid incompleteness, we cut this catalogue at $z_{phot} \leq 0.75$ and were then left with a catalogue of 6,110,921 objects, used to detect cluster candidates.

We also retrieved the magnitude catalogue of 8,485,885 objects (Annis et al. 2011) which we later cross-correlated with the photo$-z$ catalogue to obtain a complete catalogue of 4,999,968 galaxies that was fed into the Le Phare software (Arnouts et al. 1999, Ilbert et al. 2006) to compute the absolute magnitudes that we will exploit to compute Galaxy luminosity functions (GLFs).

We applied the AMACFI to our photo$-z$ catalogue. As in Adami et al. (2010), we also applied it to the Millennium simulation (Springel et al. 2005), to assess the quality of the detections and to obtain a rough estimate of the relation between the cluster masses and the significance level at which clusters were detected.

We first divided the photo$-z$ catalogue in slices of 1 deg in right ascension, to make the data manageable (in ram-active CPU memory). Each subcatalogue was then divided in slices of 0.1 in redshift. We built galaxy density maps for each redshift slice, based on an adaptative kernel technique described in Mazure et al. (2007), with 100 bootstrap resamplings of the maps to estimate correctly the background level. The pixel size was 1.002 arcmin. We then detected structures in these density maps with the SExtractor software (Bertin & Arnouts 1996) in the different redshift bins at various significance levels: 3σ, 4σ, 5σ, 6σ, and 9σ (as defined by SExtractor).

The structures were then assembled in larger structures (called *detections* in the following) using a friends-of-friends algorithm (see Adami & Mazure 1999). Two *detections* with centers distant by less than 2 arcmin (twice the pixel size defined above) were merged into a single one which was assigned the redshift of the *detection* having the highest S/N. We did not merge *detections* within 2 arcmin into a single one if their photometric redshifts differed by more than 0.09, to avoid losing clusters that could be more or less aligned along the line of sight but located at very different redshifts. The typical uncertainty on cluster positions is therefore about 2 arcmin.

In this way, we obtained a final catalogue of 956 candidate clusters detected at a significance level between 3σ and 9σ. This catalogue will be available at the VizieR interface of the Simbad database `http://vizier.u-strasbg.fr/viz-bin/VizieR`.

We extracted the objects in the S82 with a spectroscopic redshift (z_{spec}) measurement and correlated this spectroscopic catalogue with our photo-z catalogue. We found a correct agreement between z_{spec} and photo-z, with a dispersion around the 1:1 relation between 0.05 and 0.1, confirming that photo$-z$s have errors between 0.05 and 0.1.

3 The cluster characteristics

In the catalogue of 956 cluster candidates, the numbers of clusters detected at or above the various significance levels of 3σ, 4σ, 5σ, 6σ, and 9σ are: 956, 416, 219, 130, and 30.

The photometric redshift distribution of the cluster surface density (i.e. the number of clusters divided by the surface covered by our catalogue, taken to be 270 deg^2) is shown in Fig. 1 for the 956 clusters detected in S82. The median redshift of our clusters is 0.35, in good agreement with the median redshift $< z >= 0.32$ found by Geach et al. (2011) for their sample of 4098 clusters (see below). The density of detected clusters falls quite rapidly for $z > 0.4$.

As expected, there are fewer high redshift clusters detected at high ($\geq 5\sigma$) than at low (3σ and 4σ) significance level.

By applying the same detection method to the Millennium simulation, we have shown (see Adami et al. 2010, hereafter A10, Table 2) that there is a rough correspondence between the cluster detection level and its mass. We have redone the same exercise here, selecting data from the Millennium simulation and adapting them to the conditions of the S82 data analysed here, i.e. with errors on photometric redshifts between ± 0.05 and ± 0.1, a limiting redshift $z \leq 0.75$ and a magnitude limit $i \leq 21$. We find that even for the most massive haloes the percentage of detection is small: at most 25%. So all we can give is an order of magnitude: clusters detected at 3σ and 4σ have masses in the range $[10^{13} - 9 \times 10^{13}$ M$_\odot]$ while clusters detected at 6σ have masses

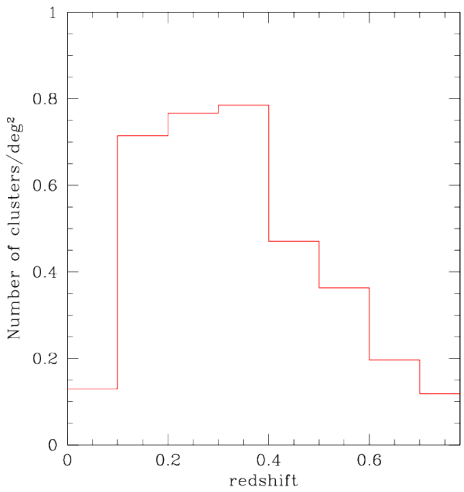

Fig. 1. Histogram of the surface density of the clusters detected in S82 in photometric redshift bins of 0.1.

in the range $[4 \times 10^{13} - 3 \times 10^{14}$ M$_\odot]$. As in A10, due to the fact that the Millennium simulation only covers an area corresponding to 1 deg^2, it includes no cluster corresponding to a 9σ detection in our study, so we cannot estimate the typical mass of the clusters detected at a 9σ level. All we can say is that these clusters must have masses larger than 10^{14} M$_\odot$.

Geach et al. (2011) detected 4098 clusters in the S82 region, but with a different definition, since they consider that a cluster begins with 5 galaxies. With this definition, it is not surprising that they detect many more clusters than us. The cross-correlation of our cluster catalogue with that of GMB, allowing a maximum identification distance of 3 arcmin, leads to 572 clusters in common. This matching radius was chosen to maximize the number of matches, taking into account the fact that the uncertainty on the cluster centers is about 2 arcmin. Out of these 572 clusters, 359 are at a redshift $z \leq 0.4$. If we consider only the 416 clusters that we detect at a significance level of 4σ or higher, 300 are at $z \leq 0.4$, and out of these 300, 225 are in common with GMB. So we can conclude that 75% of the clusters that we detect at a significance level of at least 4σ and at a redhift $z \leq 0.4$ are in common with GMB. If we now consider the clusters that we detect at a higher significance level, we find that 93% of the clusters detected at 5σ and above have a GMB counterpart, and *all* the candidate clusters that we detect at 6σ and above can be identified with a GMB cluster.

These results are satisfactory, since in spite of the differences in the methods applied to detect clusters and in the definition of what we and GMB consider as clusters, a very high percentage of the clusters that we detect at 5σ and above are also in the GMB catalogue. This means that both methods are powerful to detect the most massive clusters.

4 Properties of stacked clusters

Colour magnitude diagrams of clusters stacked in redshift bins show a red sequence, which is particularly well defined in the (r-i) versus i plot. This allows us to select cluster galaxies along the red sequence and derive GLFs. We are in the process of computing GLFs in bins of redshift but have not completed this work at the time of submission of the present contribution. All our future results will be described in a forthcoming paper (Durret et al. 2014, A&A to be submitted).

5 Morphological properties of cluster galaxies

Based on the catalogue of clusters that we have detected we have analysed statistically the morphological properties of the galaxies having a large probability of being in these clusters, i.e. for a given cluster, all the galaxies within 2 Mpc of the cluster center and with a photo$-z$ within ± 0.1 of the cluster photo-z.

To estimate the morphological properties of the galaxies, we extracted images of 4850×4850 pixels^2, with a pixel scale of 0.396 arcsec/pixel, in the g, r and i bands, around each cluster. We applied a new tool developed in SExtractor that calculates for each galaxy the respective fluxes in the bulge (spheroid) and disk. This new

experimental SExtractor feature fits to each galaxy a two-dimensional model including a de Vaucouleurs spheroid (the bulge) and an exponential disk. The PSF model used in the fit was derived with the PSFEx software (Bertin 2011) from a selection of point source images. The model fitting was carried out in the g, r, and i bands.

We applied this tool to look for differences in galaxy morphologies as a function of redshift and of significance level of the cluster detection (which is related to cluster mass) by computing for each galaxy the flux in the disk f_{disk} and that in the spheroid $f_{spheroid}$. We classified a galaxy as early type if $f_{spheroid} > f_{disk}$ and as late type if $f_{disk} \geq f_{spheroid}$. SExtractor also computes the errors on these fluxes and on the $f_{spheroid}/f_{disk}$ flux ratio.

Before stacking clusters, and searching for variations of galaxy morphologies with redshift, we made a cut in absolute magnitude in order to have comparable samples in all the redshift bins. This cut was made at $M_r \geq -19.5$, where the error on the flux ratio remains smaller than 20% for a majority of galaxies.

We limited our sample to the 416 clusters detected at a 4σ level and above, to have a sample of clusters as reliable as possible. Since no significant difference is observed between the bulge to disk decompositions in the g, r and i bands, we will only present results in the r band.

We stacked clusters in six redshift bins: $z \leq 0.15$, $0.15 < z \leq 0.25$, $0.25 < z \leq 0.35$, $0.35 < z \leq 0.45$, $0.45 < z \leq 0.55$ and $z > 0.55$ and computed the percentages of late type galaxies. If we assume that there is no observational bias due to the loss of spatial resolution for galaxies when redshift increases, we find that the percentage of late type galaxies tends to decrease with redshift, opposite to what is expected. We also stacked clusters in four bins of detection level: 4σ, 5σ, 6σ and 9σ, which roughly correspond to cluster mass bins. We find that the percentage of late type galaxies tends to increase with significance level, oppositely to what is expected (more massive clusters are expected to host more early type galaxies).

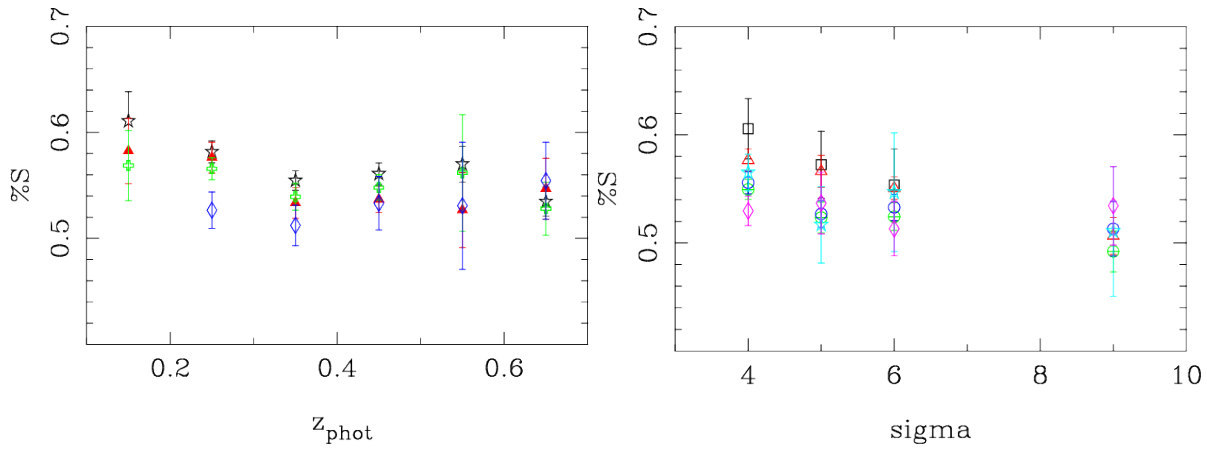

Fig. 2. Left: percentage of late type galaxies as a function of redshift, based on the bulge to disk decomposition in the r band. The data points are colour–coded as a function of detection level: black stars for 4σ, red triangles for 5σ, green squares for 6σ and blue diamonds for 9σ. **Right**: percentage of late type galaxies as a function of detection level, based on the bulge to disk decomposition in the r band. The data points are colour–coded in bins of redshift: black squares for $z \leq 0.15$, red triangles for $0.15 < z \leq 0.25$, green circles for $0.25 < z \leq 0.35$, blue circles for $0.35 < z \leq 0.45$, cyan stars for $0.45 < z \leq 0.55$, and magenta diamonds for $z > 0.55$. In both figures, the correction factors mentioned in the text have been applied.

We performed simulations to test the hypothesis that these unexpected results could be due to an observational bias. We found that, as a bias due to redshift, the percentage of late type galaxies tends to decrease with redshift and that of early types to increase. Therefore, when estimating the early type to late type ratio, a correcting factor must be applied to correct for this bias.

If we apply this correction factor (that varies with redshift), we obtain the results displayed in Fig. 2. In these two figures, error bars were taken to be Poissonian: $\sqrt{N}/N$, where N is the number of late type galaxies corresponding to each point.

We can see in these figures that the percentages of late type galaxies range between 50% and 60%. These percentages remain quite constant for $z > 0.3$, while at lower redshift they tend to decrease a little with redshift, at least in the first bin or two of significance level, except for the most massive clusters (those detected at 9σ). Comparably, the percentages of late type galaxies are found to decrease with detection level (i.e. with mass) in

the two or three bins of lowest redshift, while variations become smaller for $z \geq 0.35$.

6 Summary and conclusions

Based on the photometric redshift (hereafter photo$-z$) catalogue of Reis et al. (2012), we have searched for galaxy clusters in the Stripe 82 region of the Sloan Digital Sky Survey by applying the AMACFI cluster finder (Mazure et al. 2007). We detected 956 clusters at a 3σ level and above, in the redshift range $0.1 \leq z \leq 0.75$, with estimated mean masses between $\sim 10^{13}$ and a few 10^{14} $M_{\odot}$. A large fraction of these candidate clusters are in common with Geach et al. (2011).

The morphological analysis of the *cluster galaxies* shows that the fraction of late type to early type galaxies shows a slight increase ($\leq 10\%$) with redshift and a decrease ($\sim 10\%$) with significance level, i.e. cluster mass. This result is obtained after correcting for a bias due to the effect of increasing redshift that we quatified through simulations.

From the properties of their galaxies, the 956 candidate clusters detected here with AMACFI seem in majority to be "real" clusters, with typical cluster properties. Spectroscopic confirmation is of course necessary. It would require too much telescope time to observe all these clusters, but spectroscopic data are already available in the SDSS for some of them, and we intend to use this information in a near future. As yet another confirmation to the reality of the clusters detected in S82, we intend to identify our candidate clusters with diffuse X-ray sources detected by XMM-Newton (Takey et al. 2014).

Besides, by stacking the *cluster galaxies* in various redshift bins, we find a clear red sequence in the $(r - i)$ versus i colour-magnitude diagram, and the preliminary galaxy luminosity functions of *cluster galaxies* that we have obtained are typical of cluster GLFs. These properties make us confident that we have detected in majority *bona fide* clusters.

A comparison between our technique applied to the same data set as GMB indicates that if the candidates based on our method are 6σ detections, the sample should be well over 93% complete. In this case, the technique used to make the cluster catalog should not dominate the derivation of cosmological parameters. So AMACFI appears well adapted to search for clusters to do cosmology, though of course it should be coupled with other cluster finders to improve the robustness of detections.

We acknowledge long term financial support from CNES.

References

Adami C. & Mazure A. 1999, A&AS 134, 393
Adami C., Durret F., Benoist C. et al. 2010, A&A 509, 81
Annis J., Soares-Santos M., Lupton R.H. et al. 2011, arXiv:1111.6619
Arnouts S., Cristiani S., Moscardini L. et al. 1999, MNRAS 310, 540
Bertin E. & Arnouts S. 1996, A&A 117, 393
Bertin E. 2011, ASPC 442, 435
Geach J.E., Murphy D.N.A., Bower R.G. 2011, MNRAS 413, 3059
Ilbert O., Arnouts S., McCracken H.J. et al. 2006, A&A 457, 841
Mazure A., Adami C., Pierre M. et al. 2007, A&A 467, 49
Reis R.R.R., Soares-Santos M., Annis J. et al. 2012, ApJ 747, 59
Springel V., White S.D.M., Jenkins A. et al. 2005, Nature 435, 629
Takey A., Schwope A., Lamer G. 2014, A&A 564, 54